

MODELLING THE GALACTIC BAR USING RED CLUMP GIANTS

K. Z. Stanek¹

Princeton University Observatory, Princeton, NJ 08544–1001

e-mail: stanek@astro.princeton.edu

A. Udalski, M. Szymański, J. Kałużny and M. Kubiak

Warsaw University Observatory Al. Ujazdowskie 4, 00–478 Warszawa, Poland

M. Mateo

Department of Astronomy, University of Michigan, 821 Dennison Bldg., Ann Arbor, MI 48109–1090

and

W. Krzemiński

Carnegie Observatories, Las Campanas Observatory, Casilla 601, La Serena, Chile

ABSTRACT

The color-magnitude diagrams of $\sim 7 \times 10^5$ stars obtained for 12 fields across the Galactic bulge with the OGLE project reveal a well-defined population of bulge red clump giants. We find that the distributions of the apparent magnitudes of the red clump stars are systematically fainter when moving towards lower galactic l fields. The most plausible explanation of this distinct trend is that the Galactic bulge is a bar, whose nearest end lies at positive galactic longitude. We model this Galactic bar by fitting for all fields the observed luminosity functions in the red clump region of the color-magnitude diagram. We find that almost regardless of the analytical function used to describe the 3-D stars distribution of the Galactic bar, the resulting models have the major axis inclined to the line of sight by $20 - 30$ deg, with axis ratios corresponding to $x_0 : y_0 : z_0 = 3.5 : 1.5 : 1$. This puts a strong constraint on the possible range of the Galactic bar models. Gravitational microlensing can provide us with additional constraints on the structure of the Galactic bar.

Subject headings: stars: HR diagram – stars: statistics – Galaxy: general – Galaxy: structure

¹On leave from N. Copernicus Astronomical Center, Bartycka 18, Warszawa 00–716, Poland

1. INTRODUCTION

There is a mounting evidence that the Galactic bulge is a triaxial structure, or a bar. This was first postulated by de Vaucouleurs (1964), based on similarities between the kinematics of the gas observed towards the Galactic center and in other barred galaxies. However, the hypothesis that our Galaxy is a barred galaxy was for a long time overshadowed by “3 *kpc* expanding arm” hypothesis, despite a number of papers arguing for bar’s presence (e.g. Peters 1975; Liszt & Burton 1980; Gerhard & Vietri 1986). Only recently has the view of our Galaxy as a barred spiral gained momentum, mostly due to the work of Blitz & Spergel (1991). They analyzed 2.4 μm observations of the Galactic center and showed convincingly that the observed asymmetry in the galactic longitude distribution of surface brightness is naturally explained by the bar with the near side in the first Galactic quadrant. Binney et al. (1991) have constructed a dynamical model for gas in the inner Galaxy, and their resulting bar has the same orientation as that suggested by Blitz & Spergel (1991) in the sense that the closer part of the bar is at positive galactic longitudes. COBE-DIRBE multiwavelength observations of the Galactic center (Weiland et al. 1994) confirmed the existence of the longitudinal asymmetry discussed by Blitz & Spergel (1991). This data was used by Dwek et al. (1995) to constrain a number of analytical bar models existing in the literature.

Star counts have also shown evidence for triaxial structure in the center of the Galaxy. Nakada et al. (1991) analyzed the distribution of IRAS Galactic bulge stars and found asymmetry in the same sense as Blitz & Spergel (1991). Whitelock & Catchpole (1992) analyzed the number distribution of Mira variables in the bulge as a function of distance modulus and found that the half of the bulge which is at positive galactic longitude is closer to us than the other half. The observed stellar distribution could be modelled with a bar inclined at roughly 45 deg to the line of sight. Weinberg (1992) used AGB stars as star tracers and mapped the Galaxy inside the solar circle. He found evidence for a large stellar bar with semimajor axis of ≈ 5 *kpc* and inclination placing the nearer side of the bar at positive galactic longitudes.

A third thread of evidence comes from the gravitational microlensing towards the Galactic bulge (Udalski et al. 1994; Alcock et al. 1995; Alard et al. 1995). Observed high microlensing rate can be accounted for by stars placed in the near part of the Galactic bar microlensing the stars from the far side of the bar (Kiraga & Paczyński 1994; Paczyński et al. 1994b; Zhao, Spergel & Rich 1995). There are many implications if this scenario is correct, discussed latter in this paper. For recent reviews on the Galactic bar see Gerhard (1996) and Kuijken (1996).

In this paper we use a color-magnitude data obtained by the Optical Gravitational

Lensing Experiment collaboration for 12 fields scattered across the galactic bulge to construct the three-dimensional model of the mass distribution in the Galactic bar. The Optical Gravitational Lensing Experiment (OGLE, Udalski et al. 1993; 1994) is an extensive photometric search for the rare cases of gravitational microlensing of Galactic bulge stars by foreground stars, brown dwarfs and planets. It provides a huge database (Szymański & Udalski 1993), from which color-magnitude diagrams have been compiled (Udalski et al. 1993). Stanek et al. (1994; 1996) used the well-defined population of bulge red clump stars to investigate the presence of the bar in our Galaxy. Comparing extinction-adjusted apparent magnitudes of the red clump giants observed at fields lying at $l = \pm 5$ deg, we found that the red clump stars lying at the positive Galactic longitudes are systematically brighter by ~ 0.4 mag than the stars lying at negative l . A bar-shaped bulge whose nearer side is at the positive Galactic longitude most easily explains this offset. This agrees with Blitz & Spergel (1991) and other works.

The paper is organized as follows. In Section 2 we discuss the basis for using the red clump stars as a distance indicator. In Section 3 we discuss the data used for the bar modelling. In Section 4 we discuss various analytical models of the bar. In Section 5 we constrain these models using our data. In Section 6 we discuss various factors which might affect the fits. In Section 7 we discuss some astrophysical implications of the constructed models, among the others for the gravitational microlensing optical depth.

2. RED CLUMP GIANTS AS A DISTANCE INDICATOR

Before we model the Galactic bar using red clump stars, we shall discuss the evidence that the red clump stars would be a good distance indicator for the Galactic bulge population. Red clump stars are the equivalent of the horizontal branch stars for a metal rich population, i.e. relatively low mass stars burning helium in their cores. From stellar evolution theory (e.g. Seidel, Demarque & Weinberg 1987; Castellani, Chieffi & Straniero 1992) we expect the red clump stars to have a narrow luminosity distribution with weak dependence on age and the metallicity. For given metallicity and helium abundance, the total difference in mean clump luminosity for ages between 1 and 10 *Gyr* is ~ 0.1 mag (Seidel et al. 1987). The effect of metallicity on red clump giants luminosity and color is also relatively weak (see Sarajedini, Lee & Lee 1995, their Figs.4,5). Therefore, red clump stars form a suitable population with which to investigate the properties of high-metallicity systems, like the Galactic bulge.

Because of high and variable interstellar extinction towards the Galactic bulge, we use extinction-adjusted parameter V_{V-I} in our analysis (see Eq.1). We would like to be able

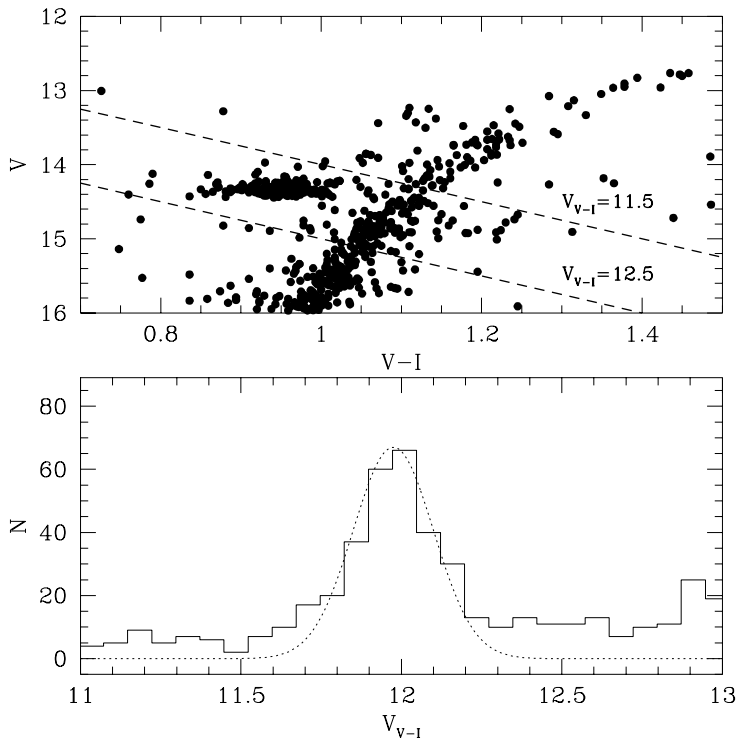


Fig. 1.— Red clump dominated part of the CMD for the globular cluster 47 Tuc (upper panel). The two dashed lines correspond to the values of the extinction-adjusted parameter V_{V-I} of 11.5 and 12.5. In lower panel we show histogram of V_{V-I} values in the vicinity of the red clump. Dashed line corresponds to a Gaussian with $\sigma = 0.12 \text{ mag}$.

to say something about the intrinsic width of the red clump population. For that, we use $V, V - I$ color-magnitude diagrams (CMDs) of the globular cluster 47 Tuc obtained by one of the authors (JK) using 2.5-meter DuPont telescope at the Las Campanas Observatory. These CMDs are described in more detail by Kałuzny & Wysocka (1996). 47 Tuc is a metal rich globular cluster with $[\text{Fe}/\text{H}] \approx -0.7$ (Zinn & West 1984) and age of 13.0 Gyr (Sarajedini et al. 1995).

We first construct a histogram of V_{V-I} values for stars in the red clump dominated region of the 47 Tuc CMD (Fig.1). The definition of the V_{V-I} parameter causes that, along with the red clumps giants we are interested in, also stars from the red giant branch which happen to have the same values of V_{V-I} are included into histogram. The resulting peak in the luminosity function is quite narrow — for comparison we plotted a Gaussian with $\sigma = 0.12 \text{ mag}$.

We want also to be able to estimate what are the effects of possible metallicity spread (McWilliam & Rich 1994; Minniti et al. 1995) on the red clump width. To do so, we selected one of Baade’s Window fields observed by OGLE, BW4, which has relatively

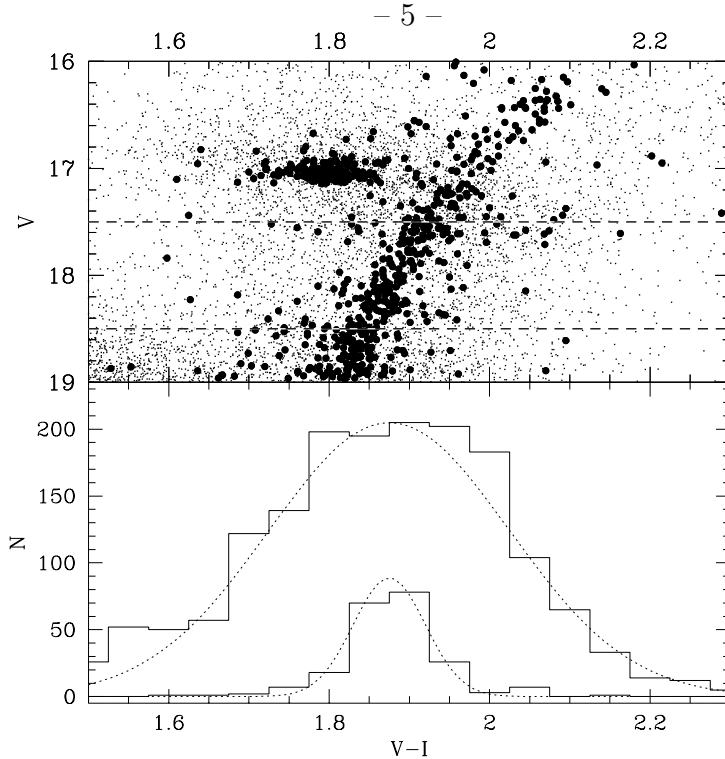


Fig. 2.— Comparison of the width of the red giant branch between the globular cluster 47 Tuc and one of the OGLE fields BW4. In upper panel we show the red clump dominated parts of both CMDs. The 47 Tuc CMD (big dots) was shifted so as to match the red clump position of the BW4 CMD (small dots). In lower panel we show histogram of $V - I$ colors for both red giant branches (limited in V by two dashed lines shown in the upper panel). The red giant branch of 47 Tuc is narrow, $\sigma \approx 0.05 \text{ mag}$, and it is much broader for the BW4 field, with $\sigma \approx 0.15 \text{ mag}$.

uniform extinction (see Stanek 1996). We then shifted the CMD of 47 Tuc to match the location of the red clumps giants in the BW4. This is shown in the upper part of Fig.2. We then plotted the histogram of $V - I$ color for red giant branch stars from both the cluster and the BW4 field (Fig.2, lower part). The red giant branch of 47 Tuc is very narrow, $\sigma \approx 0.05 \text{ mag}$, and it is much broader for the BW4 field, with $\sigma \approx 0.15 \text{ mag}$. This combined with the $\sigma = 0.12 \text{ mag}$ measured in the previous paragraph gives us the intrinsic width of the red clump giants population in the Galactic bulge $\sigma_{RC} = \sqrt{0.12^2 + 0.15^2} \approx 0.2 \text{ mag}$. We will use this number later in this paper.

3. THE DATA

We use a color-magnitude data obtained by the Optical Gravitational Lensing Experiment collaboration for 12 fields scattered across the galactic bulge to construct the 3-D model of the mass distribution in the Galactic bar. The schematic map of the fields' location in the Galactic coordinates is shown in Fig.3 and the coordinates of the fields are given in Table 1. We use 10 color-magnitude diagrams (CMDs) from Udalski et al. (1993) (fields BW1-6, MM5-B, MM7-AB, TP8) and two CMDs obtained last year specifically for the current project (fields GB11, GB13). All the data were obtained using the 1-meter Swope telescope at the Las Campanas Observatory, operated by the Carnegie Institution of Washington, and 2048×2048 Ford/Loral CCD detector with the pixel size 0.44 arcsec covering $15' \times 15'$ field of view. We did not use fields BW7 and BWC of Udalski et al. (1993) because they each contain a globular cluster, which could potentially contaminate our star counts. We also excluded fields BW8 and MM5-A because of very strong CCD bleeding columns caused by bright stars. Most of each CMD is dominated by bulge stars, with a distinct red clump, red giant, and turn-off point stars. The part of the diagram dominated by disk stars for nine BW fields was analyzed by Paczyński et al. (1994a). Stanek et al. (1994) used well-defined population of bulge red clump giants in nine BW fields and four MM fields to find an evidence for the Galactic bar. This paper is an extension of this earlier work.

To analyze the distribution of bulge red clump stars in a quantitative manner, we use the extinction-insensitive V_{V-I} parameter (Paczyński et al. 1994a; Stanek et al. 1994)

$$V_{V-I} \equiv V - 2.5 (V - I), \quad (1)$$

where we use reddening law $E_{V-I} = A_V/2.5$, following Woźniak & Stanek (1996) and Stanek (1996). The parameter V_{V-I} has been defined so that if A_V/E_{V-I} is independent of location then for any particular star its value is not affected by the unknown extinction (Woźniak & Stanek 1996). Then we consider only the region of the CMD clearly dominated by the bulge red clump stars:

$$1.5 < V - I < 2.4 \quad ; \quad 11.0 < V_{V-I} < 13.75 \quad (2)$$

For one of the fields, TP8, the average interstellar extinction is clearly lower than for the other fields, so for TP8 the selected region is:

$$1.1 < V - I < 2.0 \quad ; \quad 11.0 < V_{V-I} < 13.75, \quad (3)$$

on the other hand, for one of the new fields, GB13, the average interstellar extinction is clearly higher than for the other 11 fields, so for GB13 the selected regions is:

$$1.9 < V - I < 2.8 \quad ; \quad 11.0 < V_{V-I} < 13.75 \quad (4)$$

Table 1. Observed Fields

Field	$\alpha_{2000.0}$	$\delta_{2000.0}$	l	b	No. of RC stars
BW1	18:02:19.9	–29:49:28	1.0764	–3.5894	5,496
BW2	18:02:20.6	–30:15:18	0.7017	–3.8028	4,380
BW3	18:04:19.5	–30:15:22	0.9103	–4.1769	3,865
BW4	18:04:18.8	–29:49:12	1.2908	–3.9625	4,549
BW5	18:02:20.1	–30:02:27	0.8878	–3.6961	5,382
BW6	18:03:20.8	–30:15:10	0.8099	–3.9909	5,045
MM5–B	17:47:24.3	–34:57:38	–4.9577	–3.4479	3,844
MM7–A	18:10:52.1	–25:54:16	5.4272	–3.3385	3,572
MM7–B	18:11:39.4	–25:55:08	5.4996	–3.5008	3,493
TP8	18:17:55.0	–32:54:03	–0.0583	–7.9773	855
GB11	18:20:34.6	–23:58:45	8.1703	–4.3672	2,339
GB13	17:46:58.5	–23:01:14	5.2157	2.8113	5,144

Note. — Number of red clump stars was taken as number of stars fulfilling the inequalities (2), or (3) for the field TP8 and (4) for the field GB13.

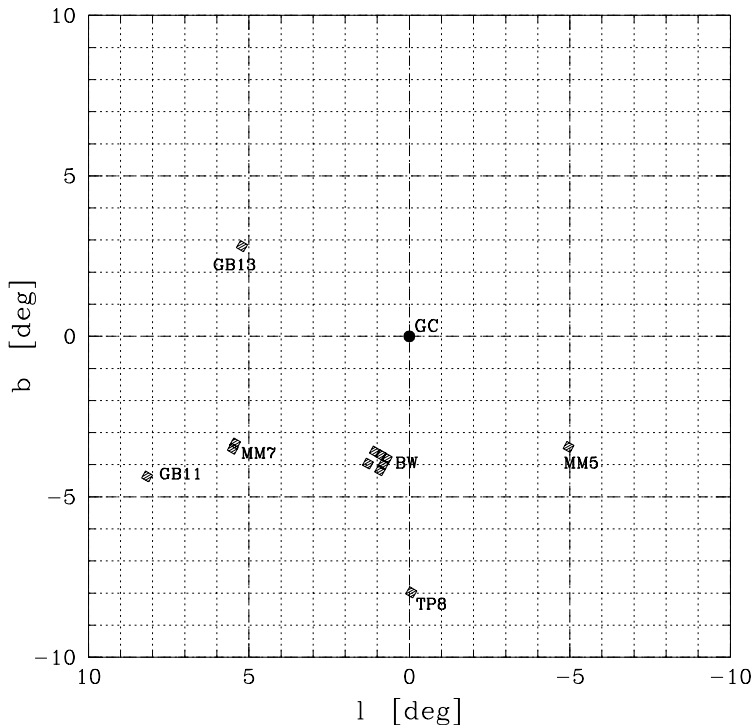


Fig. 3.— Schematic map of the 12 fields used in this paper to model the Galactic bar. The grid shown corresponds to the Galactic coordinates. GC denotes the Galactic Center, BW – Baade’s Window. For coordinates of the fields see Table 1.

Please note that in Eqs.(2–4) the range of V_{V-I} is always the same. If the value of the coefficient of the selective extinction is indeed constant throughout the Galactic bulge, as found by Woźniak & Stanek (1996), then these different selections for TP8 and GB13 fields should not affect our calculations. All stars that satisfy the inequalities (2) and (3,4) were counted in bins of $\Delta V_{V-I} = 0.05$. The result appears in Fig.4, where we see the number of stars as a function of V_{V-I} for all the fields, ordered by decreasing Galactic longitude. Please note the systematic shift between the red clump giants distribution as the l decreases, as already seen by Stanek et al. (1994; 1996). Please also note that the V_{V-I} histogram of the field GB13 is not shifted comparing to the MM7 fields, which indicates that the coefficient of the selective extinction is indeed constant throughout the Galactic bulge.

4. TRIAXIAL BAR MODELS

We seek to reproduce the observed luminosity function in each of the 12 fields (Fig.4) assuming some analytical function for the Galactic bar density distribution and fitting some simple form of the intrinsic luminosity function, the same in all the fields, for the stars in

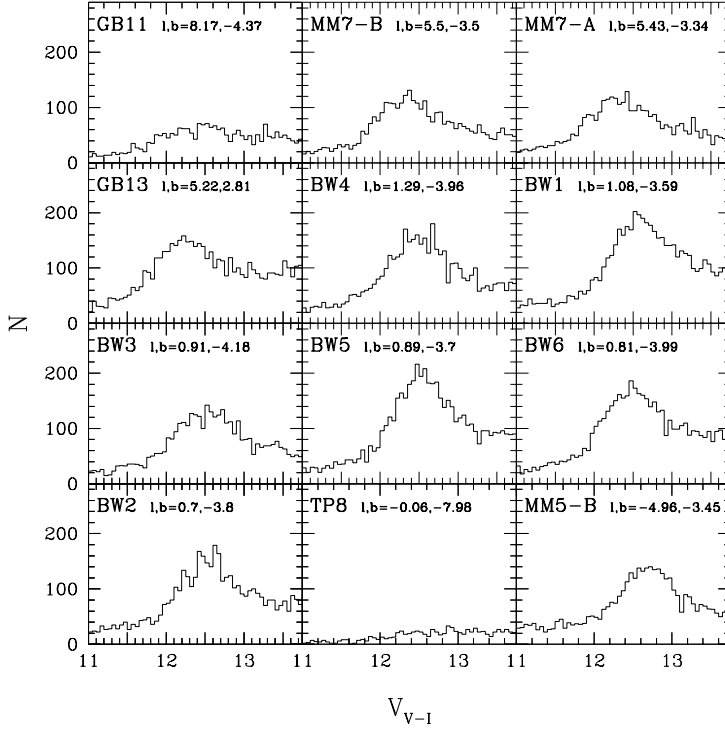


Fig. 4.— Histograms of V_{V-I} values in the red clump region (Eq.2,3,4) for all 12 fields, ordered by decreasing Galactic longitude. Please note the systematic shift, towards the larger values of V_{V-I} , between the red clump giants distribution as the l decreases – this is the bar signature already seen by Stanek et al. (1994; 1996).

the red clump region.

For the Galactic bar density distributions we follow Dwek et al. (1995) approach and select three families of the analytical functions (for detailed description see Dwek et al.):

1. *Gaussian type functions* (G), described by

$$\rho_{G1}(x, y, z) = \rho_0 \exp(-r^2/2) \quad (5)$$

$$\rho_{G2}(x, y, z) = \rho_0 \exp(-r_s^2/2) \quad (6)$$

$$\rho_{G3}(x, y, z) = \rho_0 r^{-1.8} \exp(-r^3) \quad (7)$$

2. *exponential-type functions* (E), described by

$$\rho_{E1}(x, y, z) = \rho_0 \exp(-r_e) \quad (8)$$

$$\rho_{E2}(x, y, z) = \rho_0 \exp(-r) \quad (9)$$

$$\rho_{E3}(x, y, z) = \rho_0 K_0(r_s) \quad (10)$$

3. *power-law type functions* (P), described by

$$\rho_{P1}(x, y, z) = \rho_0 \left(\frac{1}{1+r} \right)^4 \quad (11)$$

$$\rho_{P2}(x, y, z) = \rho_0 \frac{1}{r(1+r)^3} \quad (12)$$

$$\rho_{P3}(x, y, z) = \rho_0 \left(\frac{1}{1+r^2} \right)^2 \quad (13)$$

where:

$$r \equiv \left[\left(\frac{x}{x_0} \right)^2 + \left(\frac{y}{y_0} \right)^2 + \left(\frac{z}{z_0} \right)^2 \right]^{1/2} \quad (14)$$

$$r_e \equiv \left(\frac{|x|}{x_0} + \frac{|y|}{y_0} + \frac{|z|}{z_0} \right) \quad (15)$$

$$r_s \equiv \left\{ \left[\left(\frac{x}{x_0} \right)^2 + \left(\frac{y}{y_0} \right)^2 \right]^2 + \left(\frac{z}{z_0} \right)^4 \right\}^{1/4} \quad (16)$$

All these functions are allowed to be rotated in the plane of the Galaxy by the angle α , related to Dwek's et al. angle α_D by $\alpha = 90 - \alpha_D$ ($\alpha = 0$ deg corresponds to the major axis of the bar pointing at us). We also allow for the tilt out of the Galactic plane β , corresponding to Dwek's et al. angle β . We assume the distance to the center of the Galaxy 8.0 kpc .

We parametrize the fitted luminosity function in the form

$$\Phi(L) = \left(\frac{N_0}{L_\odot} \right) \left(\frac{L}{L_\odot} \right)^{-\gamma} + \frac{N_{RC}}{\sigma_{RC} \sqrt{2\pi}} \exp \left[-\frac{(L - L_{RC})^2}{2\sigma_{RC}^2} \right] \quad [L_\odot^{-1}]. \quad (17)$$

The power-law with index γ is intended to represent the underlying broad population of stars, and the Gaussian is intended to represent red clump stars. For a given V_{-I} bin, the number of stars in that bin is then given by

$$N(V_{-I}) = C_1 \int_{D_{MIN}}^{D_{MAX}} \rho(D_s) D_s^2 \Phi(L) L dD_s, \quad (18)$$

where we take $D_{MIN} = 3 \text{ kpc}$, $D_{MAX} = 13 \text{ kpc}$, C_1 is a constant, D_s is a distance from the observer to the source, and L is given by

$$L = C_2 D_s^2 10^{-0.4V_{-I}}, \quad (19)$$

C_2 being another constant. In equation (18) we assume that the number of observable stars is everywhere proportional to the density of matter and that the intrinsic luminosity function is independent of location, which gives a constant (M/L) throughout the bar.

We now have a model of the mass distribution with four or five free parameters (three axis plus one or two angles, Eqs.5-13) and the intrinsic luminosity function with four free parameters (two for the underlying power law plus two for the Gaussian red clump, Eq.17 – the intrinsic width of the Gaussian is not fitted, see below), total of 8 or 9 free parameters. We do not fit the intrinsic width of the red clump distribution σ_{RC} – we pre-set it to three values corresponding to 0.1, 0.2 and 0.3 *mag*, with 0.2 *mag* being the preferred value based on analysis in Section 2. We should mention here that the luminosity function from Eq.17 is only approximately Gaussian when transferred into magnitudes. On the other hand we have 12 fields with 55 bins in each of the fields, a total of 660 bins. This gives us number of degrees of freedom $N_{DOF} = 660 - 8 = 652$, which should be adequate to fit the model of the Galactic bar. Please note that, unlike the case of COBE-DIRBE data, we have the information about all three dimensions of the bar, but we lack COBE-DIRBE spatial coverage.

5. BAR MORPHOLOGY

Table 2 presents some of the fitted parameters in the case with the value of the assumed intrinsic width of the red clump distribution $\sigma_{RC} = 0.2$ *mag*. As we mentioned above, we also investigated cases with $\sigma_{RC} = 0.1, 0.3$ *mag* and we will discuss some aspects of this below. In all three cases we have two sub-cases: one when we allow only eight free parameters (with $\beta = 0$) and one in which we allow for the tilt out of the Galactic plane ($\beta \neq 0$).

We use χ^2 statistics as both a fitting tool, and also as a relative measure of the quality of each of the models. As we discuss later in this paper, our best fit models have values of the $\chi^2/N_{DOF} \approx 2.3$, which indicates that χ^2 should not be used as a measure of absolute goodness of the fit. We therefore do not give formal errors of the fitted parameters in Table 2 based on usual χ^2 confidence levels.

5.1. Comparison between the models

Before we start discussing triaxial bar models, we should mention that we also tried to fit axially-symmetric set of models, described by the same functions as the triaxial bars, but

Table 2. Parameters of the Best-Fit Bar Models for $\sigma_{RC} = 0.2 \text{ mag}$

Model	α [deg]	β [deg]	x_0 [pc]	y_0 [pc]	z_0 [pc]	χ^2/N_{DOF}
G1	24.6	...	1514	691	463	2.60
	24.5	0.5	1529	676	460	2.60
G2	24.9	...	1239	609	438	2.90
	23.9	2.4	1293	565	423	2.84
G3	24.8	...	3851	1698	1114	2.43
	24.7	-0.1	3857	1705	1115	2.43
E1	20.7	...	1665	691	297	2.47
	20.1	-0.1	1680	704	296	2.47
E2	23.8	...	899	386	250	2.37
	23.8	0.0	897	387	250	2.37
E3	23.9	...	854	381	278	2.59
	24.0	0.4	857	376	276	2.59
P1	22.7	...	724	299	189	2.27
	22.6	-0.2	738	308	194	2.27
P2	22.6	...	1056	435	275	2.27
	22.4	-0.2	1061	443	278	2.27
P3	22.8	...	1400	580	368	2.27
	22.7	-0.2	1389	582	368	2.27

Note. — For every model two cases are shown: first with 8 free parameters and second with $\beta \neq 0$ (9 free parameters).

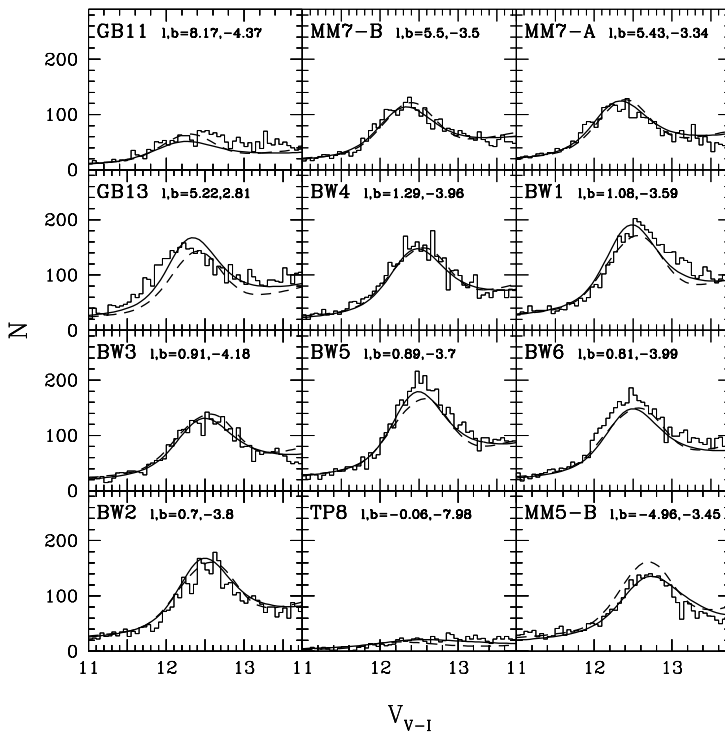


Fig. 5.— The same histograms as in Fig.4, but with the best (P1 – continues line) and worst (G2 – dashed line) model fits shown. The assumed value of the intrinsic width of the red clump for the fits is $\sigma_{RC} = 0.2 \text{ mag}$.

with x_0 set to be the same as y_0 . Not surprisingly, axially symmetric models fitted our data substantially worse than triaxial models, with the best fit model achieving $\chi^2/N_{DOF} \approx 3.1$ compared to $\chi^2/N_{DOF} \approx 2.3$ for the best triaxial models.

From Table 2 we can immediately see that none of the models fits the data perfectly, i.e. χ^2/N_{DOF} is relatively high. We discuss possible reasons for that in Section 6. Still, some analytical functions fit better than others. We find that the whole class of power-law models (P1, P2, P3) gives us the best fits to the data, for all three values of the σ_{RC} investigated. However, the values of χ^2/N_{DOF} for other analytical functions, especially for the G3 and E2 models, are not much worse than for the power-law models. What is somewhat surprising is that the G2 model is our “worst fit” model, given that this was Dwek et al. best fit model. We will discuss agreement of our work with the analysis of COBE-DIRBE data in Section 7.

To illustrate how significant the differences are between the best and the worst fit models, in Fig.5 we show the same histograms as in Fig.4, but with the best (P1 – continues line) and worst (G2 – dashed line) model fits shown. For some of the fields, like GB13 or MM5-B, these differences are easily noticeable.

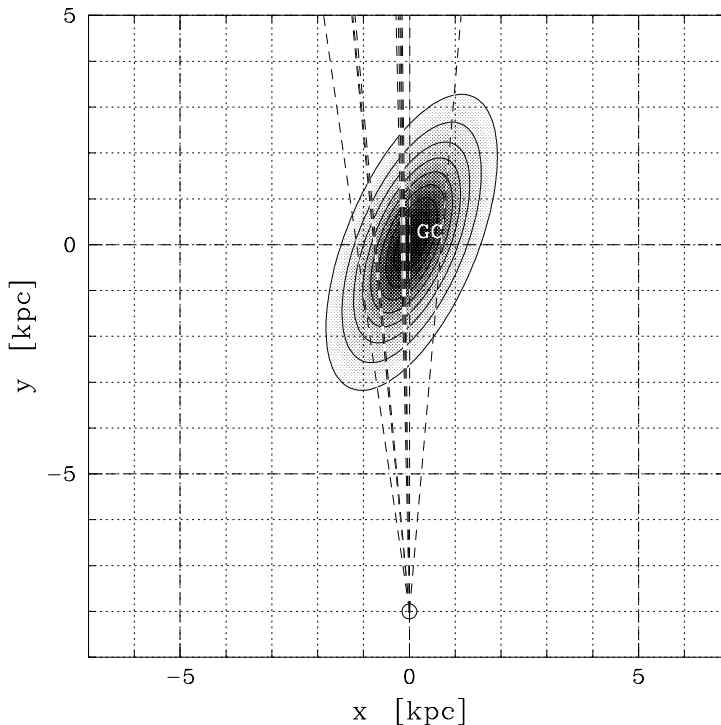


Fig. 6.— Cut through the “recommended” E2 model at 700 pc below the Galactic plane, i.e. at the galactic latitude $b = -5$ deg at the distance of 8 kpc . With dashed lines we show the lines of sight for the 12 fields used in this paper. Contours start at 10% of the central value and increase by 10%.

In Fig.6 we show a cut through the E2 (our “recommended” model of the Galactic bar, see Section 7.1) model at 700 pc below the Galactic plane, i.e. at the galactic latitude $b = -5$ deg at the distance of 8 kpc . With dashed lines we show the lines of sight for the 12 fields used in this paper. Contours start at 10% of the central value and increase by 10%. As we discuss below, this figure would be similar for other analytical functions used.

5.2. Orientation of the Galactic bar

The characteristic angles of the fitted models (α, β) are defined in the same way for each model, so there is possible direct comparison between the models. As can be seen from Table 2, the tilt angle β is never important in reducing the χ^2 values significantly. Also, except for the G2 model, angle β is always smaller than 1 deg. We will therefore set $\beta = 0$ deg in further discussion.

To analyze the behavior of the angle α we plot in Fig.7 the value of this angle for

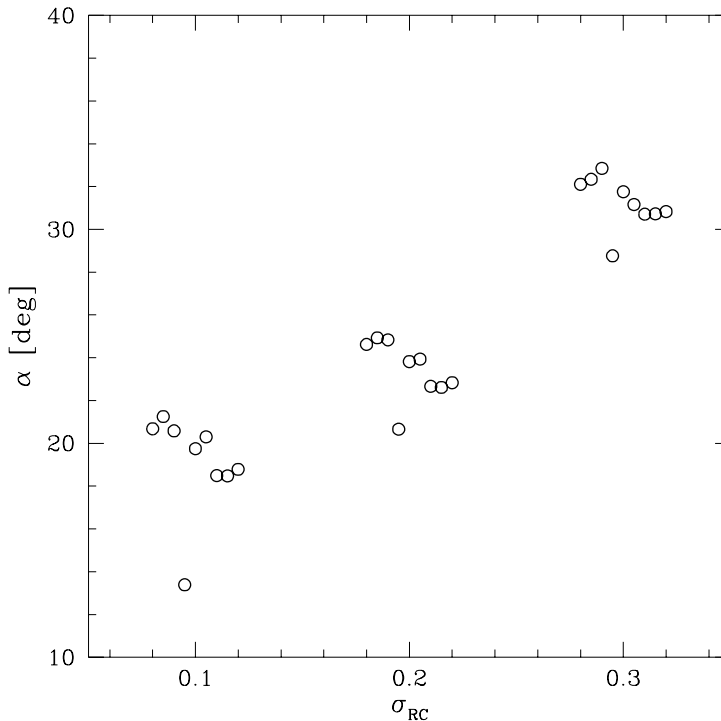


Fig. 7.— The inclination angle for the various models at the assumed width of the red clump $\sigma_{RC} = 0.1, 0.2, 0.3 \text{ mag}$. The horizontal spread along the x -axis for each σ_{RC} was done for the clarity.

various models as the function of the assumed σ_{RC} . The horizontal spread along the x -axis for each σ_{RC} was done for the clarity of presentation. It is immediately clear from Fig.7 that for a given σ_{RC} the values of α are very similar between the models (see also Table 2). Even for the E1 model, which has the most discrepant value of α comparing to other models, this value is still only few degrees below the other values. Also, there is visible in Fig.7 clear trend in the sense that for larger σ_{RC} given analytical model has larger inclination angle α . This trend was to some extent expected: to fit the observed data, the models with larger σ_{RC} have to have smaller depth along the line of sight, which for triaxial objects decreases with increasing inclination angle. For the preferred value of $\sigma_{RC} = 0.2 \text{ mag}$ (Section 2) the inclination angle is between $\alpha \approx 20 - 26 \text{ deg}$. Even taking the most extreme values of α from Fig.7 we find that the inclination angle is between $\alpha \approx 14 - 34 \text{ deg}$. This is a very good constraint comparing to the values of α found in the literature (for discussion see Dwek et al. 1995; Gerhard 1996; Kuijken 1996). Our result agrees roughly with Dwek’s et al. range of $\alpha \approx 0 - 40 \text{ deg}$, with an average of $\alpha \approx 25 \text{ deg}$. In our case, however, constraints on the value of α are much better due to the nature of the data used, which, unlike the COBE-DIRBE data, contains the third dimension information in the form of the shift between the red clump giants distributions (Fig.4).

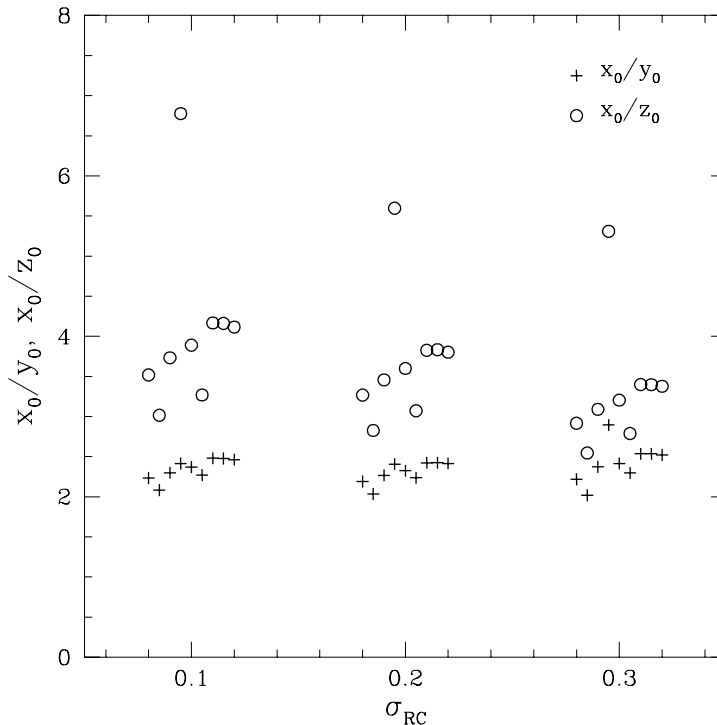


Fig. 8.— The axis ratios $x_0/y_0, x_0/z_0$ for the various models at the assumed width of the red clump $\sigma_{RC} = 0.1, 0.2, 0.3 \text{ mag}$. The horizontal spread along the x -axis for each σ_{RC} was done for the clarity.

5.3. Bar axis ratios

Unlike the characteristic angles, the scale lengths for different functional forms cannot be compared directly. We can however compare the axis ratios for various models. In Fig.8 we show the axis ratios $x_0/y_0, x_0/z_0$ for the various models at the assumed width of the red clump $\sigma_{RC} = 0.1, 0.2, 0.3 \text{ mag}$. The horizontal spread along the x -axis for each σ_{RC} was done for the clarity of the presentation, as in Fig.7.

Let us first discuss the ratio x_0/y_0 , i.e. the ratio of the bar major axis to the minor axis lying in the plane of the Galaxy. This ratio for all the models does not change significantly with σ_{RC} and is between 2.0 – 2.4, except for the E1 model with $\sigma_{RC} = 0.3 \text{ mag}$, for which $x_0/y_0 = 2.9$. This is a very tight constraint, again much tighter than $x_0/y_0 \approx 3 \pm 1$ obtained by Dwek et al. from COBE-DIRBE data (see also their Fig.5).

On the other hand, there is a clear trend between x_0/z_0 and σ_{RC} in the sense that for larger σ_{RC} given analytical model has smaller axis ratio x_0/z_0 . This was somewhat expected: as we increase the σ_{RC} , x_0 must decrease to fit the data, but we expect that z_0 would remain approximately the same, since z_0 is the scale length perpendicular to the

plane of the Galaxy and it is not strongly affected by “rotating” the bar. Also, the scatter of x_0/z_0 for different models is bigger than in case of x_0/y_0 . For the preferred value of $\sigma_{RC} = 0.2 \text{ mag}$, x_0/z_0 is between 2.8 – 3.8, again with the exception of E1 model, for which it is $x_0/y_0 \approx 5.6$.

Judging from the map of the observed fields (Fig.3), one could be worried that most of the constraint we have on the z_0 comes from the TP8 field, in which there are very few red clump stars (Fig.4 and Table 1). This is however not the case: even within Baade’s Window there is a clear gradient, in the number of the red clump stars, with the distance from the Galactic center. The BW1 field has about 40% more red clump stars than the BW3 field. In fact, we run a series of fits without the TP8 field and the resulting models were very close to what we present in this paper.

5.4. Models with centroid offset

There is evidence from the gas kinematics pointing to the fact that the centroid of the gas emission from the Galactic bar is offset at $l \approx 0.5 \text{ deg}$ (Blitz 1995; Weinberg 1996). We decided to add to our models one additional parameter δl which allows for the offset of the centroid of the Galactic bar in the l direction. In Table 3 we list the best fit parameters of the resulting models, and also compare the χ^2/N_{DOF} for models with the offset and without it.

It is interesting to note that all the models prefer to have positive δl , in agreement with Blitz (1995). Also, for some models, most noticeably the G2 model, introducing this additional parameter reduced χ^2/N_{DOF} considerably. This is not simply an effect of having one additional parameter – the tilt angle β had hardly any effect on our models. We conclude by saying that our results are suggestive of a small ($\delta l \approx 0.5 \text{ deg}$) centroid offset of the Galactic bar.

One could in principle introduce another additional parameter describing the centroid offset in the b direction. With current data, however, we have only one field at positive Galactic latitude, which provides very little lever arm to constrain an offset in b . We thus make no attempt to include it in our models.

6. FACTORS AFFECTING THE FITS

In the previous section we fitted various analytical models to the luminosity function of the bulge red clumps stars and obtained the parameters of the 3-D mass distribution of

Table 3. Parameters of the Best-Fit Bar Models with the Centroid Offset

Model	α [deg]	δl [deg]	x_0 [pc]	y_0 [pc]	z_0 [pc]	χ^2/N_{DOF} <i>with offset</i>	χ^2/N_{DOF} <i>no offset</i>
G1	24.1	0.60	1575	663	477	2.46	2.60
G2	24.1	0.82	1325	560	452	2.64	2.90
G3	23.9	0.53	4028	1656	1155	2.33	2.43
E1	19.1	0.24	1745	723	303	2.47	2.47
E2	23.5	0.46	935	385	262	2.29	2.37
E3	23.2	0.51	904	376	293	2.44	2.59
P1	22.5	0.18	784	321	207	2.26	2.27
P2	22.4	0.17	1095	448	288	2.26	2.27
P3	22.7	0.27	1486	606	396	2.25	2.27

Table 4. Agreement of the Bar Models with the Artificial Data

Model	α [deg]	x_0 [pc]	y_0/x_0	z_0/x_0	χ^2/N_{DOF}
E2	20.0	1000	1:2.00	1:2.50	1.11
G1	18.1	1478	1:1.96	1:2.42	1.19
G2	17.8	1298	1:1.87	1:2.27	1.28
G3	19.2	4537	1:1.97	1:2.63	1.09
E1	13.8	1650	1:1.90	1:3.48	1.40
E2	18.3	1000	1:1.98	1:2.58	1.07
E3	18.0	1075	1:1.91	1:2.43	1.12
P1	19.2	1565	1:2.00	1:2.69	1.14
P2	19.4	2653	1:2.01	1:2.72	1.16
P3	18.6	1869	1:1.99	1:2.62	1.08

the Galactic bar. This procedure is subject to possible various systematic errors, which we discuss in some detail below.

6.1. Bad selection of fitted models

One obvious disadvantage of the whole procedure described in the previous section is that we fit only a number of selected analytical functions describing the 3-D light (mass) distribution of the Galactic bar. Indeed, high value of the formal χ^2 we obtained even for our best-fit model – P1 with $\sigma_{RC} = 0.2 \text{ mag}$ and 8 free parameters has $\chi^2/N_{DOF} = 2.27$ – suggests that we either underestimate our errors (which were taken to be Poissonian \sqrt{N}) or the Galactic bar 3-D mass distribution is described by some other triaxial function or most probably is only roughly described by an analytical function. Nevertheless, by following Dwek et al. approach and fitting a whole set of different analytical functions with different properties we showed we can retrieve successfully at least some of the Galactic bar properties. For example, it is clear from Fig.7 that the inclination angle of the bar to the line of sight α does not depend strongly on the model we fit and is affected stronger by the assumed value of the intrinsic width of the red clump σ_{RC} .

To investigate to some extent how strong the effect of fitting an improper analytical function is on the fitted parameters, we generated artificial random histograms of the V_{V-I} distributions using the E2 model. We then fitted this artificial data using all nine different analytical functions used in this paper. In Table 4 we show both the parameters of the input model (first row) and the fitted parameters of all nine models. For reasons discussed in the previous section, instead of y_0, z_0 scale lengths we show the axis ratios $y_0/x_0, z_0/x_0$, as these are more relevant for comparing the agreement between the models.

As can be seen in Table 4, agreement in the fitted inclination angle is very good. The E1 model deviates most from the input $\alpha = 20 \text{ deg}$, but this is also true when fitting to the real data. This only reconfirms our strong conviction that we can constrain the inclination angle α of the bar very well. The y_0/x_0 axis ratio is also recovered remarkably well. As to the z_0/x_0 axis ratio, except for the E1 model, it is also well recovered by all other models. We conclude by saying that all the models we use, except for the E1 model, can be used to recover the parameters of the Galactic bar with similar fidelity.

6.2. Red clump detection efficiency

It is possible that we detect red clump giants with different efficiency among the 12 fields we use in this paper. This could affect some of the parameters we fit, some stronger than others, for example inclination angle of the bar probably would not depend very strongly on this effect, but the axis ratios probably would. Red clump stars we use in our analysis are always well above the detection threshold, $3 - 4 \text{ mag}$ in V , so we do not expect a strong variation in efficiency among the fields. Looking at fields which are adjacent (like BW1 and BW5 or the two MM7 fields) we generally find that the histograms of V_{V-I} values are similar for these fields (Fig.4 and Table 1).

There are two levels on which stars can be lost: the CCD detection and the construction of a CMD from I and V databases. Udalski et al. (1993) addressed the question of CCD star detection efficiency by placing artificial stars on the CCD and then retrieving them through the standard OGLE data pipeline. They found that the CCD detection efficiency in the interesting us magnitude range is roughly constant and is about $\sim 80\%$, which would not change the parameters of the fit we are interested in. We therefore make no correction for the CCD detection efficiency. The other reason that some stars are not included in the CMD is that the star photometry is not good enough to pass a corresponding criterion. Udalski et al. (1993) used rather stringent photometric quality constrains on what stars can qualify to be included in the CMD, so only about 60% of stars from the I, V databases are finally included. These constrains are however the same for all the fields, so we neglect that in our fitting procedure.

6.3. Effects of interstellar extinction

One can imagine that a large scale gradient in the reddening law could explain the systematic shift of the red clump giants in magnitude with the galactic longitude, which we discuss in this and earlier works (Stanek et al. 1994; 1996). This would cause V_{V-I} defined by Eq.1 to be invalid globally. However, Woźniak and Stanek (1996) found no such gradient. What they could not exclude were smaller variations of this coefficient among various fields, but again, inspection of Fig.4 shows a good agreement in red clump peak position for fields located at the approximately same position, like the BW fields. Even fields MM7 and GB13, located at approximately the same galactic l , but on opposite sides of the Galactic plane (Table 1), have practically the same red clump peak position (Fig.4), even that the GB13 field has somewhat higher extinction then the MM7 fields.

6.4. Galactic disk contamination

As we select a region of the CMD and then use all stars in this region to construct a luminosity function, we may expect some contamination from stars located in the Galactic disk. Stanek et al. (1994) considered this problem using Bahcall & Soneira (1980) model of the Galactic disk and found the contamination to be negligible (see Stanek’s et al. Fig.2). This is because in the region corresponding to red clump giants we expect only either bright and nearby, or evolved disk stars, of which there are very few.

A related problem: our star counts could also be contaminated by stars from the metal poor stellar spheroid. We do not account for this population, having already 8–9 free parameters in our fit. However, this should be negligible, just as was contamination by disk stars. Red clump becomes weak quite rapidly, as seen from V_{V_I} histogram of the fields GB11 and TP8, i.e. metal rich Galactic bar star counts, in the region of the CMD we select for our analysis, strongly dominate.

6.5. Metallicity gradient in the Galactic bulge

There seems to be a small metallicity gradient throughout the Galactic bulge (Minniti et al. 1995; but see McWilliam & Rich 1994), which could shift a little intrinsic color and luminosity of the red clump stars across the bulge. For all the models we took that into account by assuming

$$V_{V-I,RC} = V_{V-I,0} + \kappa \times \begin{cases} r \\ r_s \\ r_e \end{cases} \quad (20)$$

where the choice of r, r_s or r_e depends on the density model fitted.

We found that this additional parameter did not improve significantly the quality of the fits, we therefore did not present in Table 2 the models with $\kappa \neq 0$.

7. ASTROPHYSICAL IMPLICATIONS OF BEST-FIT MODELS

7.1. Agreement with COBE-DIRBE data

The analytical models we used in this work were identical to those used by Dwek et al., so we should be able to compare our results directly (with the remainder that the angle α we use differs from Dwek et al. α_D by $\alpha \equiv 90 - \alpha_D$). For comparison we use Dwek et

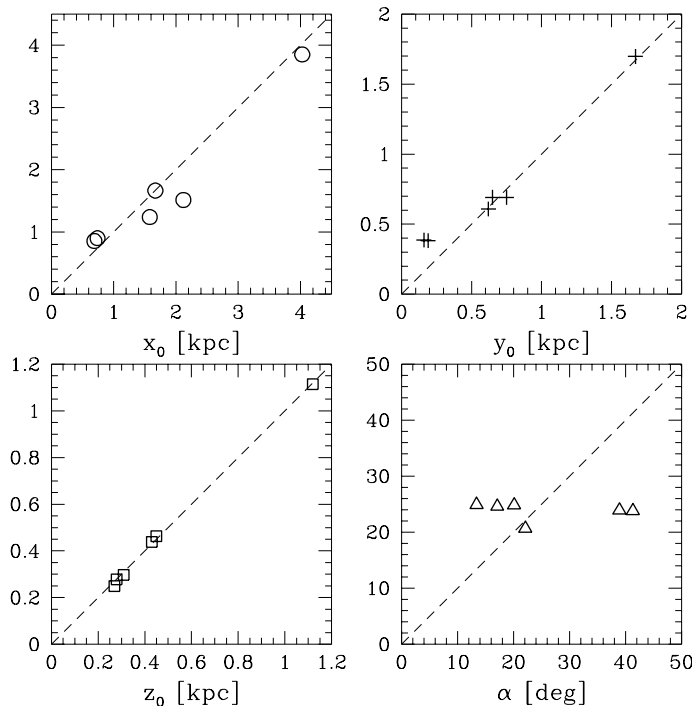


Fig. 9.— The values of x_0, y_0, z_0, α from Dwek et al. (x -axis) and from our work (y -axis). The dashed lines correspond to these values being equal.

al. best fitting models at $2.2 \mu\text{m}$ with cutoff at 5 kpc , the same cutoff we use in this paper (Eq.18). The Dwek et al. fitting procedure (their Table 1) does not like power-law models (our best fit models), so here we will only compare six other models we both used.

In Fig.9 we plot the values of x_0, y_0, z_0, α from Dwek et al. (x -axis) and from this work (y -axis). The dashed lines correspond to these values being equal. There is a very good agreement between the values of z_0 found by Dwek et al. and those we find: they can be compared directly using Dwek et al. Table 1 and our Table 2. This is extremely reassuring because z_0 is not affected by “rotating” the bar, so the fact that we both get essentially the same values for z_0 means that, although here we are using data of entirely different nature from COBE-DIRBE data, we probe in our analysis the same stellar populations.

The correlations between x_0, y_0 values are not nearly as good as for z_0 , but still rather clear. On the other hand, there is no correlation between the inclination angles α obtained by Dwek et al. and our values. As we discussed earlier in this paper, regardless of the fitted model we obtain almost the same value for this angle, but Dwek et al. obtained a wider range of values for this angle. We are confident that the nature of the data we use in this work allows for much better constraint of this parameter than the 2-D COBE-DIRBE infrared intensity maps.

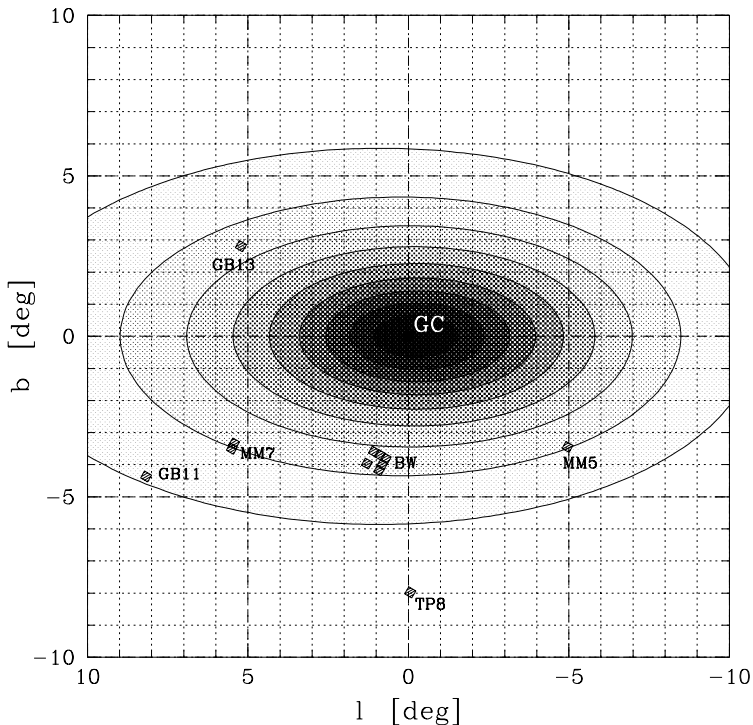


Fig. 10.— Map of the projected light from the “recommended” E2 model in the inner 20×20 deg region of the Galaxy, with our fields also shown. Contours start at 10% of the central value and increase by 10%.

As we mentioned in Section 5, the G2 model which was Dwek et al. best fit model fits our data worst. There is however several models which seem to fit both COBE-DIRBE and our data reasonably well. In fact, for the G3 model the values of the bar parameters obtained by Dwek et al. (their Table 1) are remarkably similar to ours (Table 2). The E2 model also fits reasonably well in both cases, and we suspect that if the value of α for this model was fixed by Dwek et al. to our value of $\alpha \approx 24$ deg, the agreement between x_0, y_0 would be much better. According to the trends we discussed in Section 5, lowering α from Dwek et al. 41 deg to our 24 deg would increase both x_0 and y_0 to values closer to ours. The E2 model might be preferred over the G3 model as it fits better the COBE-DIRBE data in the inner region of the Galaxy, where we do not have the CMD data from a low extinction fields.

To summarize, for those who want to use a Galactic bar model which should not be grossly wrong over large range of galactocentric distances, we recommend the E2 exponential model with *our* values for the bar parameters: $\alpha = 24$ deg; $x_0 = 900$ pc; $y_0 = 385$ pc; $z_0 = 250$ pc. In Fig.10 we show the projected light from this model for the inner 20×20 deg region of the Galaxy, with our fields also shown.

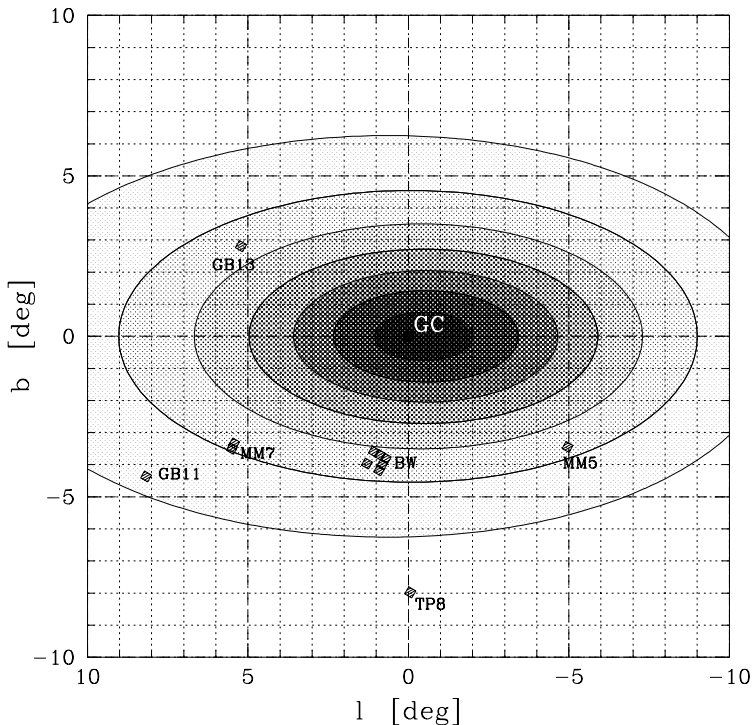


Fig. 11.— Map of the microlensing optical depth τ produced by the “recommended” E2 model in the inner 20×20 deg region of the Galaxy, with our fields also shown. The mass of the Galactic bar was assumed to be $M_{bar} = 2 \times 10^{10} m_{\odot}$. Contours start at $\tau = 5 \times 10^{-7}$ and increase also by $\tau = 5 \times 10^{-7}$ up to 3.5×10^{-6} . The contribution to the optical depth from the Galactic disk was not included.

Contours start at 10% of the central value and increase by 10%. The asymmetry between the positive and negative l sides of the Galactic bar is visible, but not striking.

7.2. Microlensing phenomena due to the Galactic bar

Microlensing can provide us with additional information on the properties of the Galactic bar. As noticed first by Kiraga & Paczyński (1994), stars in the Galactic bulge lensing other stars in the bulge produce significant contribution to the microlensing optical depth, comparable to that produced by the Galactic disk stars lensing bulge stars. This effect is strongly enhanced when the Galactic bulge is a bar with the major axis inclined to the line of sight by less than 45 deg (Paczynski et al. 1994b; Zhao et al. 1995). Recently Zhao & Mao (1996) investigated in detail how different models of the Galactic bar would differ in the optical depth for microlensing they produce, so here we want to show only some of the aspects of the microlensing by the Galactic bar.

In Fig.11 we show a map of the microlensing optical depth τ produced by our “recommended” E2 model in the inner 20×20 deg region of the Galaxy, with our fields also shown. The mass of the Galactic bar was assumed to be $M_{bar} = 2 \times 10^{10} m_{\odot}$. Contours start at $\tau = 5 \times 10^{-7}$ and increase also by $\tau = 5 \times 10^{-7}$ to the maximum of $\tau = 3.5 \times 10^{-6}$. The contribution to the optical depth from the Galactic disk was not included. Details of this microlensing map would be different if we used one of other models discussed in this paper, but the overall effect of the optical depth dropping off rapidly with the distance from the Galactic center, faster along the minor axis, would remain. As discussed by Zhao & Mao (1996), some few hundred microlensing events are needed before the microlensing can really make the difference for the existing Galactic bar models. Fortunately, this is very feasible judging from the existing microlensing experiments observing the Galactic bar (Udalski et al. 1994; Alcock et al. 1995; Alard et al. 1995; Alcock et al. 1996).

Another aspect of the microlensing by the Galactic bar was first noticed by Stanek (1995). As can be deduced from Fig.6, the stars from the far side of the Galactic bar will be preferentially lensed if most of the lensing comes from the bar stars (Paczynski et al. 1994b; Zhao et al. 1995). This leads to the offset in the brightness of the lensed stars, as compared to all observed stars, discussed in detail by Stanek (1995). The value of this offset correlates very well with the depth of the Galactic bar along the line of sight (Stanek 1995, his Fig.3). About a hundred of microlensing events in the red clump region of the CMD are needed to measure this effect with desired accuracy.

8. SUMMARY

In this paper we have used color-magnitude data obtained by the OGLE collaboration for 12 fields scattered across the galactic bulge (Fig.3) to construct the three-dimensional model of the mass distribution in the Galactic bar. We model the Galactic bar by fitting for all fields the observed luminosity functions in the red clump region of the color-magnitude diagram (Fig.4, 5). We find that almost regardless of the analytical function used to describe the 3-D stars distribution of the Galactic bar, the resulting models are inclined to the line of sight by $20 - 30$ deg (Fig.7), with axis ratios corresponding to $x_0 : y_0 : z_0 = 3.5 : 1.5 : 1$ (Fig.8). This puts a strong constraint on the possible range of the Galactic bar models.

Comparing our result with the results of Dwek et al. (1995), we find a good agreement between the derived parameters of the models (Fig.9), but we constrain the bar parameters much tighter. We recommend as a model which fits well both COBE-DIRBE and our data the E2 model (Eq.9) with the values for the bar parameters: $\alpha = 24$ deg; $x_0 = 900$ pc; $y_0 = 385$ pc; $z_0 = 250$ pc. We show various properties of this model

in Fig.reffig6, 10, 11. Gravitational microlensing can provide us with additional constraints on the structure of the Galactic bar.

The text of this paper along with the figures in PostScript format is available using anonymous ftp on `astro.princeton.edu`, in `stanek/Barmodel` directory.

We would like to thank B. Paczyński for constant advice and many stimulating discussions. W. Colley once again helped us to “polish” the text. KZS was supported by the NSF grant AST 9216494 to Bohdan Paczyński and also with the NAS Grant-in-Aid of Research through Sigma Xi, The Scientific Research Society. AU, MSz and MK were supported with Polish KBN grant 2P03D02908 and JK was supported with Polish KBN grant 2P03D00808.

REFERENCES

- Alard, C., et al., 1995, *The Messenger*, 80, 31
- Alcock, Ch., et al., 1995, *ApJ*, 445, 133
- Alcock, Ch., et al., 1996, *ApJ*, accepted (<http://xxx.lanl.gov/abs/astro-ph/9512146>)
- Binney, J., Gerhard, O. E., Stark, A. A., Bally, J., & Uchida, K. I., 1991, *MNRAS*, 252, 210
- Blitz, L., 1996, in *IAU Symp.* 169, ed. L. Blitz, in press
- Blitz, L., & Spergel, D. N., 1991, *ApJ*, 379, 631
- Castellani, V., Chieffi, A. & Straniero, O., 1992, *ApJS*, 78, 517
- Dwek, E., et al., 1995, *ApJ*, 445, 716
- de Vaucouleurs, G., 1964, in *IAU Symp.* 20, eds. F. J. Kerr & A. W. Rodgers, p.195
- Gerhard, O. E., & Vietri, M., 1986, *MNRAS*, 223, 337
- Gerhard, O. E., 1996, in *IAU Symp.* 169, ed. L. Blitz, in press (<http://xxx.lanl.gov/abs/astro-ph/9604069>)
- Kałużny, J., & Wysocka, A., 1996, in preparation
- Kiraga, M., & Paczyński, B., 1994, *ApJ*, 430, L101
- Kuijken, K., 1996, in *IAU Coll.* 157, eds. R. Buta, D. A. Crocker & B. G. Elmegreen, p.504
- Liszt, H. S., & Burton, W. B., 1980, *ApJ*, 236, 779
- McWilliam, A., & Rich, M. R., 1994, *ApJS*, 91, 749

- Minniti, D. Olszewski, E. W., Liebert, J., White, S. D. M., Hill, J. M., & Irwin, M. J., 1995, *MNRAS*, 277, 1293
- Paczyński, B., Stanek, K. Z., Udalski, A., Szymański, M., Kałużny, J., Kubiak, M., & Mateo, M., 1994a, *AJ*, 107, 2060
- Paczyński, B., Stanek, K. Z., Udalski, A., Szymański, M., Kałużny, J., Kubiak, M., Mateo, M., & Krzemiński, W., 1994b, *ApJ*, 435, L113
- Peters, W. L., 1975, *ApJ*, 195, 617
- Sarajedini, A., Lee, Y. W., & Lee, D. H., 1995, *ApJ*, 450, 712
- Seidel, E., Demarque, P., & Weinberg, D., 1987, *ApJS*, 63, 917
- Stanek, K. Z., 1995, *ApJ*, 441, L29
- Stanek, K. Z., 1996, *ApJ*, 460, L37 (<http://www.aas.org/ApJ/v460n1/5793/5793.html>)
- Stanek, K. Z., Mateo, M., Udalski, A., Szymański, M., Kałużny, J., Kubiak, M., 1994, *ApJ*, 429, L73
- Stanek, K. Z., Mateo, M., Udalski, A., Szymański, M., Kałużny, J., Kubiak, M., Krzemiński, W., 1996, in *IAU Coll. 157*, eds. R. Buta, D. A. Crocker & B. G. Elmegreen, p.545
- Udalski, A., Szymański, M., Kałużny, J., Kubiak, M., & Mateo, M., 1993, *Acta Astron.*, 43, 69
- Udalski, A., Szymański, M., Stanek, K. Z., Kałużny, J., Kubiak, M., Mateo, M., Krzemiński, W., Paczyński, B., & Venkat, R., 1994, *Acta Astron.*, 44, 165
- Weiland, J. L., et al., 1994, *ApJ*, 425, L81
- Weinberg, M. D., 1992, *ApJ*, 384, 81
- Weinberg, M. D., 1996, in *IAU Colloquium 157*, eds. R. Buta, D. A. Crocker & B. G. Elmegreen, p.516
- Whitelock, P., & Catchpole, R., 1992, in: “The Center, Bulge, and Disk of the Milky Way”, ed. L. Blitz, p.103
- Woźniak, P. R., & Stanek, K. Z., 1996, *ApJ*, to appear in June 10 issue (<http://xxx.lanl.gov/abs/astro-ph/9509040>)
- Zhao, H. S., Spergel, D. N., & Rich, M. R., 1995, *ApJ*, 440, L13
- Zhao, H. S., & Mao, S., 1996, *MNRAS*, submitted (<http://xxx.lanl.gov/abs/astro-ph/9605030>)
- Zinn, R. J., & West, M. J., 1984, *ApJS*, 55, 45